Shape optimization of a hydrofoil with leading-edge protuberances using full factorial sweep sampling and an RBF surrogate model

Amin Nazemian[1], Parviz Ghadimi[2]

Amirkabir University of Technology, Department of Maritime Engineering
Tehran, Iran, e-mail: [1] anazemian@aut.ac.ir, [2] pghadimi@aut.ac.ir
corresponding author

Abstract

This paper investigates improving the leading-edge of a hydrofoil with sinusoidal protuberances based on its hydrodynamic performance. The original hydrofoil geometry was inspired by the leading edge of the flipper of a humpback whale. A multi-step optimization process was performed for a 63_4-021 hydrofoil. The free-form deformation technique defined the shape parameters as a variable design, and these parameters included the amplitude of the leading-edge protuberances, which ranged from 0 to 20% of the chord length, and the corrugate span, with 3 and 4 crests. The flow characteristics of a parametric hydrofoil were examined using a CFD solver, and the lift, drag, and lift-to-drag ratio (L/D) were computed as responses to the optimization cycle. To accomplish this, two design study methods were sequentially applied at different angles of attack. A full factorial design sweep tool was applied that went through all parameter value combinations, and an RBF-based surrogate model was constructed to investigate the system behavior. The results indicated the existence of an optimum design point, and the highest L/D ratio was determined to be 10.726 at a 12° angle of attack.

Introduction

Many studies have used shape optimization to increase the efficiency of hydrofoils, and inspiration from nature has helped engineers improve their designs. The agility of humpback whales arises due to the leading-edge protuberances on their pectoral flippers, termed tubercles (Fish & Battle, 1995; Fish, 1999). Tubercles have an effect similar to the phenomenon in which large raised bumps on the leading edge of a wing increase its aero/hydrodynamic performance. Fish and Battle (Fish & Battle, 1995) found that the mean cross-section of the flippers has an aspect ratio of 6 and a profile similar to a sinusoidal NACA 63_4-021 airfoil. They also outlined how to add similar extensions to the leading edge in terms of the amplitude and wavelength. The effect of additional parts on the performance of foils had only

been previously studied in a few prior studies (Norberg, 1990; Bushnell & Moore, 1991; Wu, Vakili & Wu 1991). Bushnell (Bushnell & Moore, 1991) showed that humpback whale fin protuberances control the flow, maintain the lift at high attack angles, and reduce drag. Watts and Fish (Watts & Fish, 1999) conducted bumped airfoil experiments in both water and wind tunnels and determined that tubercles on the leading edge of an airfoil increased lift by 4.8%. Further numerical computations confirmed this result and indicated that the presence of tubercles decreased the effects of drag by 40%.

After the experimental research by Miklosovich et al. (Miklosovich et al., 2004), the study of humpback whale fins accelerated. By using wind tunnel tests, Miklosovich et al. compared two humpback whale fin models – one with and one without tubercles – and they reported a 6% increase over the

baseline of maximum lift and a 40% delay in the stall angle of attack for the flipper model with protuberances; however, using this inactive flow control method is not always suitable. As Stein and Murray (Stein & Murray, 2005) showed, at angles of attack between 8° and 12°, an airfoil with a protuberance leads to a significant loss of lift and increased drag, which causes a sharp decrease in the lift-to-drag ratio (L/D). Johari et al. (Johari et al., 2007) examined the airflow of a NACA 63_4-021 airfoil in 6 different modes by varying the amplitude and wavelength of a sinusoidal leading-edge to calculate the lift, drag, and pitching moment. They compared it to basic foil at angles of attack between 6° and 30°, and their results indicated better performance for hydrofoils with various protuberances in the post-stall angle of attack region. They also indicated that amplitude changes in the leading edge were more effective in foil performance than their wavelength changes.

However, Hansen et al. (Hansen, Kelso & Dally, 2011) showed that the effect of different tubercle amplitudes on the performance of the foil depended on the angle of attack and was not permanent. Although the results of a study by Hansen et al. were related to two airfoils other than NACA 63_4-021, Cai et al. (Cai et al., 2015) showed that the effect of protuberances on an airfoil's leading edge was nearly the same in different foils. In different research conducted by Johari (Johari, 2012), the effect of the Reynolds number on an original and leading-edge modified NACA 63_4-021 was evaluated. The results showed that the stall angle and the maximum lift coefficient of the baseline foil increased with the Reynolds number, up to 3.6×10^5. In contrast, the Reynolds number played only a minor role in establishing the lift and drag characteristics of foils with a modified leading edge.

The dependence of the behavior of sinusoidal wavy leading-edge foils on the Reynolds number has recently been experimentally investigated by Peristy et al. (Peristy et al., 2016) on NACA 0018. Their study indicated that a lift force reduction at small attack angles and an increase in the drag due to the creation of bumps on the leading edge raised doubts as to whether this method was suitable for controlling a foil's behavior. Despite the complex performance of an airfoil's leading edge with protuberances, a consensus has been reached that using this method to control passive flow only improves performance at certain angles of attack. In this regard, Zheng et al. (Zhang, Wang & Xu, 2013; 2014) also examined one of the models defined by

Johari et al. (Johari et al., 2007) and showed that improvements in the performance using this model occurred only at post-stall angles of attack. Another innovative experimental work was reported by Custodio et al. (Custodio, Henoch & Johari, 2012), in which the effect of leading-edge tubercles on an airfoil's efficiency was examined. It was found that the spanwise flow between protuberances caused interactions between them that generated a bi-periodic flow pattern, demonstrating the effect of the aero/hydrodynamic performance of the foils.

Numerical investigations on flow control have been used to investigate an airfoil's behavior. Numerical simulations have some advantages when using low and high Reynolds flow patterns to explain complex phenomena (Pedro & Kobayashi, 2008; Weber et al., 2011; Dropkin et al., 2012). Pedro and Kobayashi (Pedro & Kobayashi, 2008) performed a numerical investigation on the separation phenomenon and improved the performance of a modified foil with leading-edge protuberances using detached eddy simulations (DESs) and concluded that performance improvements were due to an increase in flow-induced vertices and a delay in the trailing-edge separation. Dropkin et al. (Dropkin et al., 2012) and Weber et al. (Weber et al., 2011) applied the Spalart–Allmaras turbulence model to compute the aerodynamic forces of an airfoil with sinusoidal leading-edge protuberances. Similarly, Skillin et al. (Skillin et al., 2015) determined the cause of a stall delay by examining the flow around a tubercled airfoil and also showed that a wavy airfoil obtained higher lift at post-stall angles. Paula et al. (de Paula et al., 2017) experimentally investigated the presence of wavy bumps on the leading edge of a very thick airfoil, and the results confirmed an improvement in the stall situation in these wings. On the other hand, Custodio et al. (Custodio, Henoch & Johari, 2018) reported some tunnel tests for semi-span hydrofoils that had an underlying NACA 63_4-021 profile with rectangular and a swept leading edge tubercled geometry. The effect of cavitation phenomena was analyzed at different angles of attack.

Based on the outlined literature review, almost all research has been conducted on flow patterns around foils with sinusoidal leading-edge protuberances, and the details of foil performance and the mechanism of the leading-edge protuberances on flow control have been discussed. However, shape optimization of hydrofoils with sinusoidal leading edges, and particularly the interactions between design variables, has not yet been addressed. Therefore, in this paper, the sensitivity of the shape parameters in

the leading-edge region was analyzed by considering the main airfoil inspired by a humpback whale fin, i.e., NACA 63$_4$-021. By using a full factorial sweep design study and RBF-based surrogate model, the hydrodynamic performance of the foil was improved. To accomplish this, an integrated computational tool was used as an efficient and fast convergence application to construct an optimization process. A free-form deformation (FFD) technique was first applied for CAD parametrization. The defined tubercled hydrofoil parameters consisted of the control point's position of every crest and trough in the chord direction. The defined objective function was the lift-to-drag ratio (*L/D*), and FFD geometry control points were used as variables that were introduced to the CFD solver. The developed optimization framework determined the position of these control points to improve the objective, and the results of the modified leading-edge shape were presented and analyzed.

Problem definition

The goal of this paper is to apply a design study process to optimize the amplitude and wavelength of the protuberances on the leading-edge of a NACA 63$_4$-021 foil using the experiment described by Johari et al. (Johari et al., 2007) as a reference. Parameters X1 and X2 are defined as global parameters that adjust the movements of FFD control points along the chord. Shape modification and changes to the leading-edge form accomplished by the 7 points were regularly moved by adding X1 and X2 from 0 to −0.02 m (Figure 1). As an example, Figure 2 presents a modified hydrofoil obtained by adjusting different values of X1 and X2 to create a sinusoidal leading-edge profile along the spanwise direction with different amplitudes and different numbers of crests. The crest-to-crest distance of a wavy edge is defined as the wavelength, which is 0.5c here.
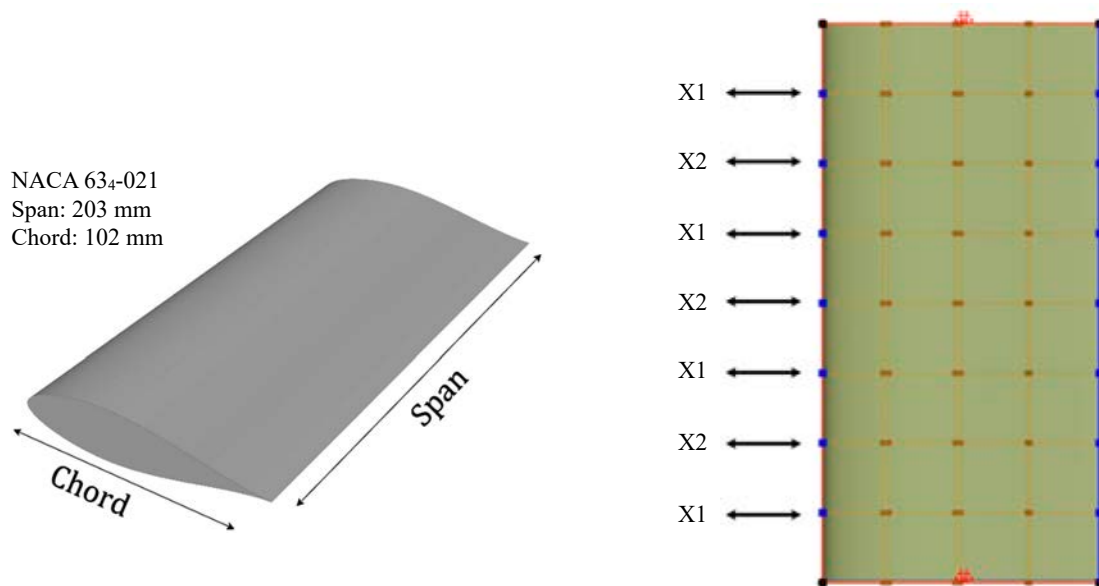

Figure 1. Baseline hydrofoil (foil with no protuberances; X1 = 0, X2 = 0) and design variables (X1, X2)

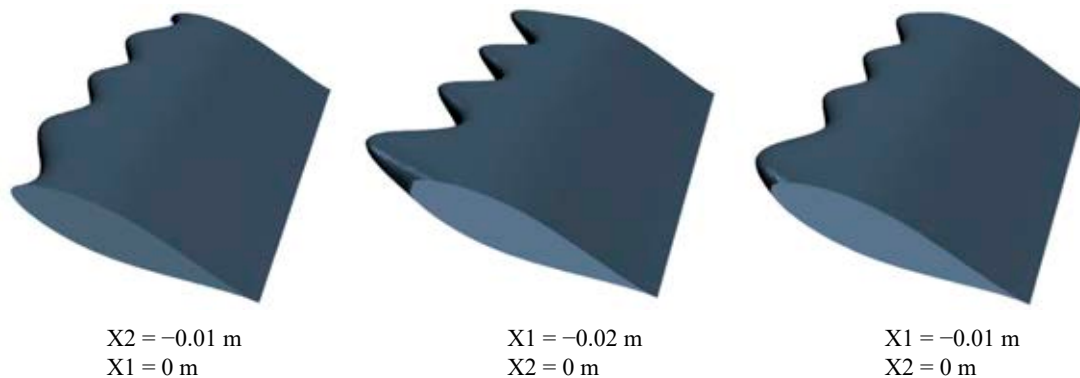| X2 = −0.01 m | X1 = −0.02 m | X1 = −0.01 m |
| X1 = 0 m | X2 = 0 m | X2 = 0 m |

Figure 2. Different values of X1 and X2 resulting in different amplitudes and leading-edge shapes
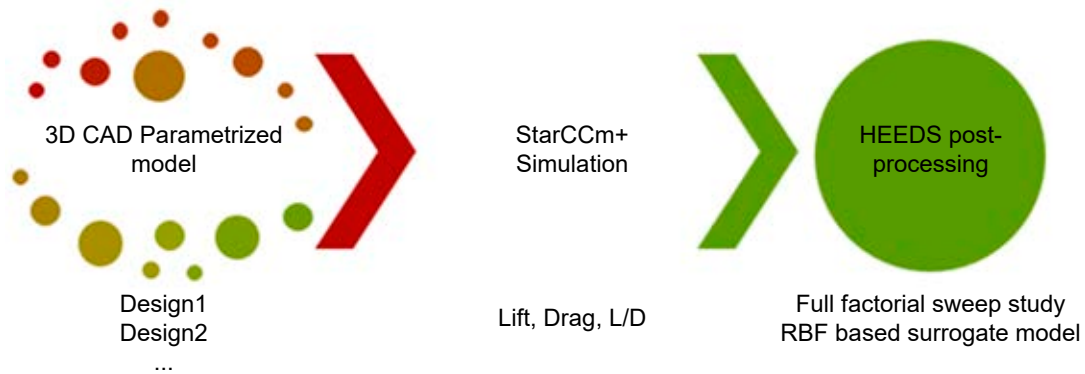
Figure 3. Flowchart of the design study process

Design study process

In this section, the overall design study process is introduced, followed by a description of its modules, geometry parameterization, numerical simulation set up, and design data modelling. In this study, we used a surface modification technique based on FFD to define local variations in the hydrofoil geometry during the design study. The objective of this study was to obtain the ultimate shape optimization of a sinusoidal leading-edge by calculating the lift, drag, and lift-to-drag ratio, and maximizing L/D. Numerical simulations were performed with the RANSE-based CFD solver within StarCCM+ software. All geometries extracted from CAD design were connected to simulations via HEEDS software at angles of attack of 6°, 9°, 12°, 15°, 18°, and 21°. To examine the sensitivity and effectiveness of the variables, an RBF-based interpolation was used to estimate the system's response to help assess the best design base at higher L/D ratios. Figure 3 shows the flowchart of the design study process.

Numerical setup

This study used the RANS equation solver within StarCCM+ to simulate a fully-submerged leading-edge corrugated hydrofoil at a constant velocity and uniform flow of 1.8 m/s and at different angles of attack. A physical model was selected based on the StarCCM+ user guide (User Guide, 2020). An implicit unsteady scheme was used for temporal discretization, while utilizing the SIMPLE algorithm to couple the pressure and velocity equations. The selected turbulence model for the current study is the standard k-ε model, which has been extensively used in industrial applications and similar studies (User Guide, 2020).

An unstructured trimmer mesh was used for mesh operation, in which the width of the computational domain was equal to the foil span. Symmetrical plane conditions were applied along the y-axis, which implies that a nominal 2D foil performance was investigated, without considering the effects of tip vortices. To avoid blockage effects, the boundaries of the computational domain were smoothly extended, as shown in Figure 4a. The prism layers and additional wall functions were applied to resolve the boundary layer at the hull. The height of the first boundary layer around the foil was set to 0.02 mm, making the maximum y^+ values < 5. The hydrofoil surfaces were defined as no-slip walls. At the inlet boundary, the velocity components were specified. At the outlet boundary, the outlet pressure boundary
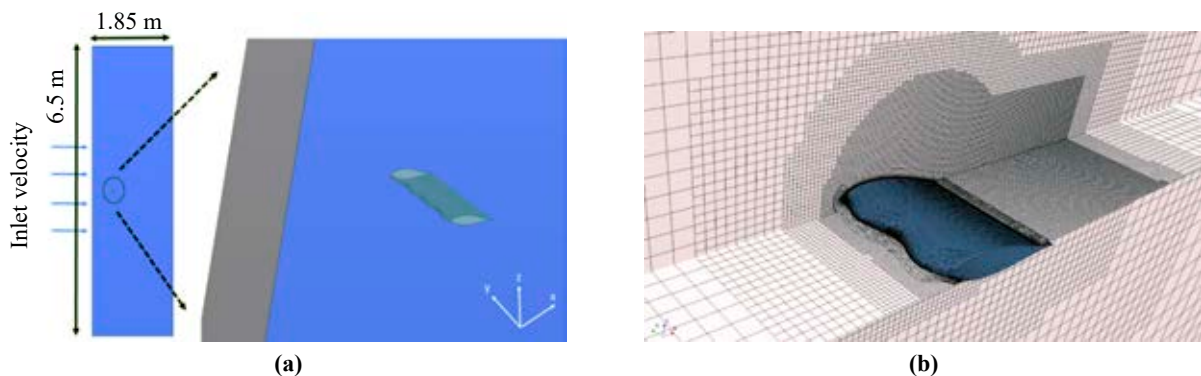

Figure 4. Computational domain and boundaries (a), and unstructured trimmer mesh around the hydrofoil (b)

condition was prescribed, while at the top and bottom of the domain, a symmetrical boundary condition was applied. Figure 4a shows the computational fluid domain and its boundaries. To capture flow patterns and sharp edges, surface and volumetric refinements were applied to the volume mesh. Figure 4b displays the selected mesh characteristics for a baseline hydrofoil (with no protuberance) at 6° and 24° angles of attack (Johari et al., 2007). A mesh study was used to select an appropriately-sized base mesh cell. Mesh refining and grid convergence were continued until the solutions were independent of the mesh size.

Mesh sensitivity analysis

To determine the optimum mesh size with acceptable numerical accuracy and appropriate element numbers, mesh convergence studies were carried out using a speed of 1.8 m/s. A mesh convergence study was conducted by changing the values of the lift and drag coefficient, as presented in Figure 5. The initial mesh size was a 4% chord length, and four mesh planes were made according to a 45% refinement ratio. As shown in Figure 5, the difference between grid 3 and grid 4 was not significant; therefore, the full mesh independence reached about 4.25 million cells, and grid 3 was selected as the optimum mesh plan. The lift and drag coefficients are defined as follows:

$$C_L = \frac{L}{\frac{1}{2}\rho U_\infty^2 cs} \qquad (1)$$

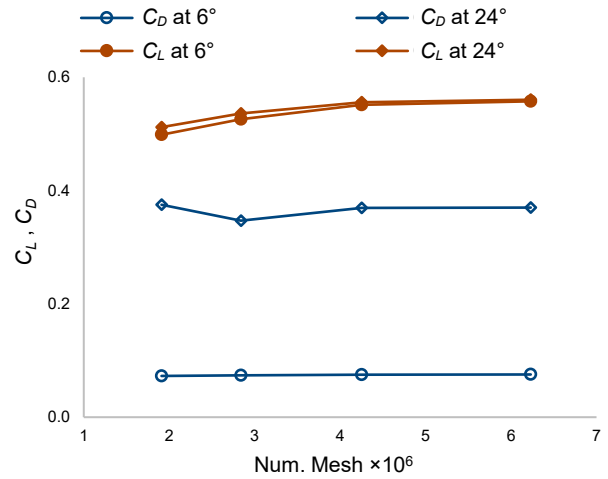$$C_D = \frac{D}{\frac{1}{2}\rho U_\infty^2 cs} \qquad (2)$$

Figure 5. Mesh element number baseline airfoil

where L and D are the lift and drag of the hydrofoil, respectively; ρ is the density of the fluid; U_∞ is the inflow velocity; c is the baseline chord; and s is the foil span. A vorticity contour streamlined around the modified hydrofoil is displayed in Figure 6.

Results and discussion

Design exploration was conducted to analyze the key parameters that affect the product's performance. There are two main categories in the design exploration process: performance assessment and design optimization. A performance assessment study runs a product through a pre-defined set of conditions to understand the influence of important parameters on a product's performance. In a design optimization study, an optimization algorithm automatically determines the input conditions to improve the product with respect to a specific goal. Since these two categories provide different kinds of information,
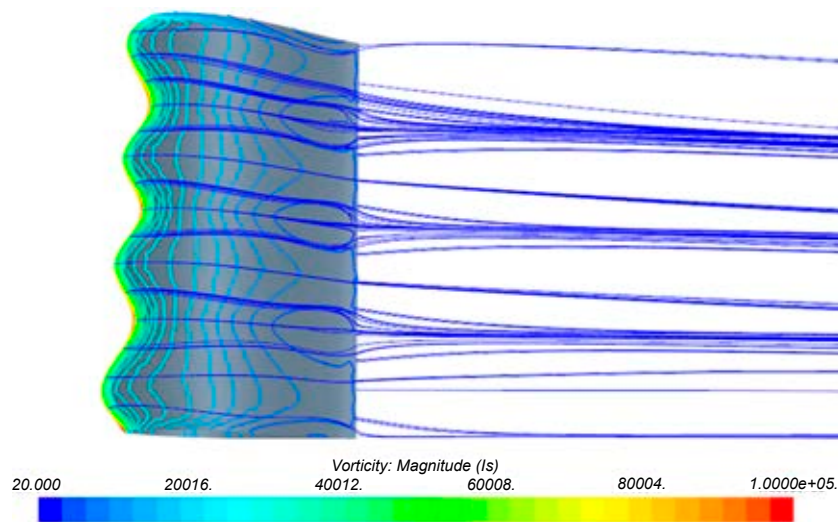

Figure 6. Vorticity contour line with streamline around a modified hydrofoil

a constructive and efficient design exploration process is usually a combination of both (User Guide, 2020).

Accordingly, for performance assessment, the sweep sampling technique is adopted to distribute 216 design points in the design space to generate data. The generated geometries consist of [6 angles of attack ×6 X1 points ×6 X2 points], and then the *L/D* ratio was calculated for these hydrofoils. The sweep sampling was represented graphically with a response surface method in Figure 7a at 6°, 9°, 12° angles of attack, and in Figure 7b at 15°, 18°, 21° angles of attack. To better understand the system behavior, an adapted design optimization algorithm based on RBF surrogate was applied to analyze the results to determine the optimum design. Consequently, inputs and outputs were prepared to fit a surrogate model, which can be developed without significant expense compared with the cost of acquiring data from the response surface. After the RBF surrogate model was constructed, cross-validation was performed to examine the accuracy of the model. The basic idea of cross-validation was to leave out one sample point and then predict it using the model built by the remaining sample points. The difference

between the exact value of the objective function at the given sample point (obtained by the CFD tool) and the approximate value of the objective function at the given sample point (predicted by the RBF surrogate model) is then calculated. If the difference is small enough, the model is valid; otherwise, if the difference is large, the number of sampling points is increased and the CFD calculation for new samples is repeated. Figure 8 shows the cross-validation of these models that indicate the validity of interpolation because the residual value of cross-validation is 0.966.

As shown in Figure 7, cutting the planes at different angles of attack represent regions where the observable target is predicted to be higher than other parts of the parameter domain. The *L/D* of the optimum design was about 10, and *L/D* values at 9° and 12° angles of attack were higher than others. At most angles of attack, the value of *L/D* was maximized if the values of X1 and X2 were in the lower part of their range. If X1 and X2 were zero, the shape of the hydrofoil would be its baseline form; therefore, the protuberances reduced the lift-to-drag ratio at different angles of attack and variable values. However, some small regions require a deeper investigation.
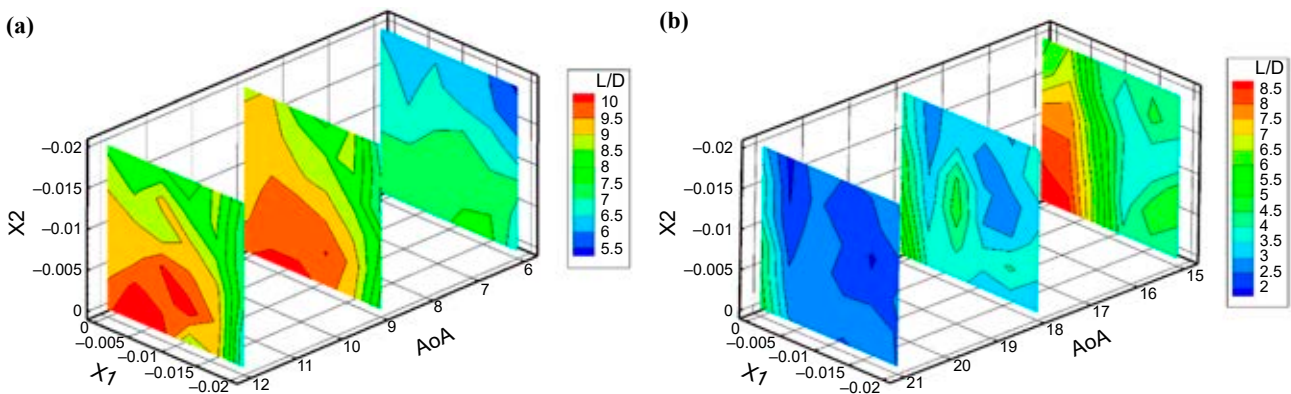

Figure 7. Cutting plane of design space based on response of the *L/D* ratio: [AoAs: 6°, 9°, 12°] (a), [AoAs: 15°, 18°, 21°] (b)
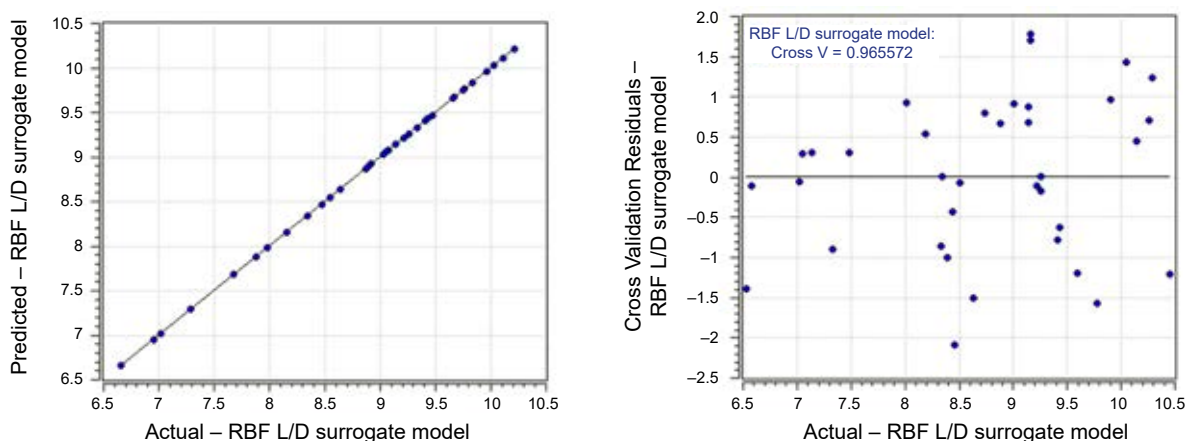

Figure 8. Cross validations of the surrogate model; cross-validation of residuals = 0.966
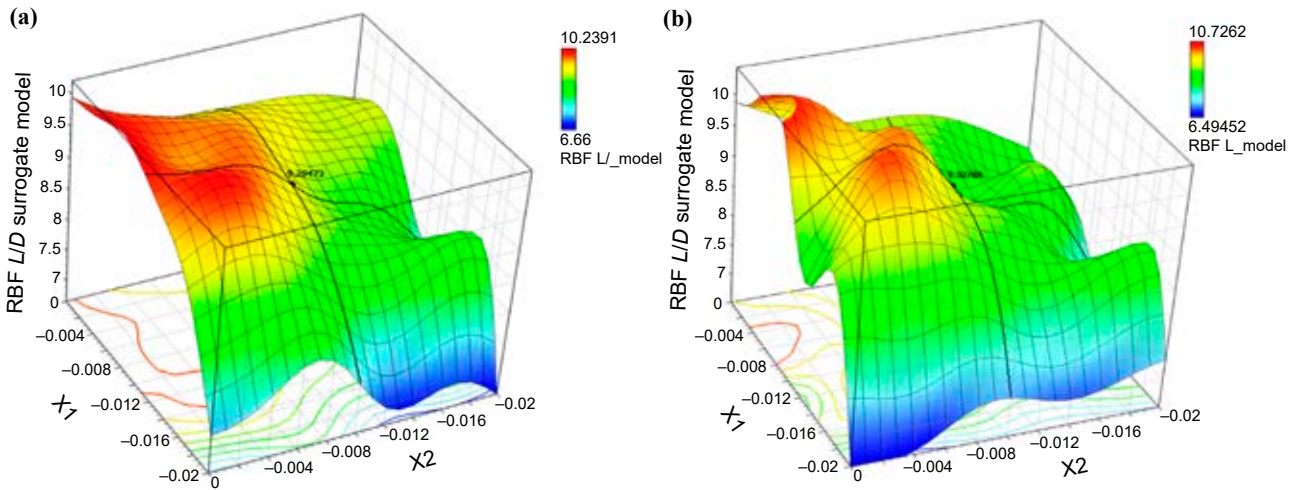
(a)

(b)

Figure 9. 3D response surface for design parameters (*X1, X2*) and response (*L/D*) at AoA: 9° (a) and 12° (b)

The results of the 3D response surface of the RBF surrogate model for the input design parameters (X1, X2) are presented in Figure 9 for 9° and 12° angles of attack. The *L/D* in a small region can be substantially increased due to the protuberances. A comparison between 4 crests with large (4L) and medium (4M), and 3 crests with large (3L) and medium (3M) sinusoidal leading-edge amplitudes is presented in Figure 10, which shows the *L/D* values at different angles of attack (6°–24°). The values of the parameters of the under-studied modified hydrofoils are presented in Table 1.
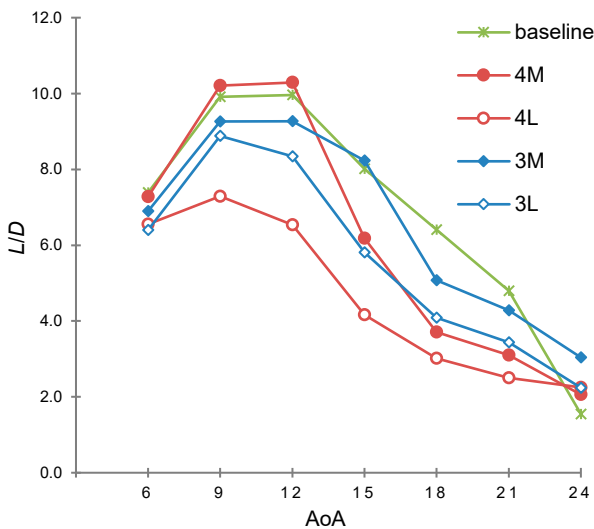

Figure 10. Comparison of *L/D* at different angles of attack

Table 1. Parameter values of the under-studied modified hydrofoils

Name	X1 [m]	X2 [m]
4L	−0.02	0
4M	−0.008	0
3L	0	−0.02
3M	0	−0.008

Based on the data interpolation of the surrogate model, the highest *L/D* ratio of 10.726 was obtained using X1 = −0.006 m and X2 = 0 and a 12° angle of attack. The sinusoidal leading-edge with 4 medium-sized (4M) crests had a higher *L/D* ratio than the wavy edge with 3 crests at a low angle of attack. At a higher angle of attack, the *L/D* ratio plots converged, and this ratio decreased until *L/D* of the baseline became lower than the modified hydrofoil (at a 24° AoA). As a result, the *L/D* of hydrofoils with protuberances on the leading-edge increased in the post-stall region. Another achievement is that the 3M tubercled hydrofoil obtained higher *L/D* ratios at higher angles of attack. The improved performance of the 3M form of the modified hydrofoil indicates there is an optimum design for tubercled hydrofoils.

Conclusions

In this paper, a design study process was developed based on three fundamental disciplines. The free-form deformation (FFD) technique was first applied for CAD parametrization, i.e., geometry reconstruction discipline. The constructed geometries were then introduced into the CFD solver as the second discipline to evaluate the lift-to-drag ratio (objective function). The last discipline included a sweep design study and an RBF-based surrogate model that was applied for design exploration. This was done to identify an optimum design and sensitivity of the shape parameters in the leading-edge region. Inspired by humpback whale fins, i.e., NACA 63$_4$-02, the hydrodynamic performance of a foil with sinusoidal leading-edge protuberances was analyzed.

The presented optimization framework determined the control point positions to improve the

objective. The design parameters of the tubercled hydrofoil included the control point's position of every crest and trough in the chord direction (X1 and X2). Different forms of the sinusoidal leading edge were constructed by varying X1 and X2. A comparison of the constructed geometries at different angles of attack indicated that there is an optimum design for tubercled hydrofoils. The highest *L/D* ratio was determined to be 10.726 when X1 = −0.006 m and X2 = 0 at a 12° angle of attack.

Acknowledgment

References

1. Bushnell, D.M. & Moore, K.J. (1991) Drag reduction in nature. *Annual Review of Fluid Mechanics* 23, pp. 65–79.
2. Cai, C., Zuo, Z., Liu, S. & Wu, Y. (2015) Numerical investigations of hydrodynamic performance of hydrofoils with leading-edge protuberances. *Advances in Mechanical Engineering* 7 (7).
3. Custodio, D., Henoch, C. & Johari, H. (2012) *Aerodynamic Characteristics of Finite-Span Wings with Leading Edge Protuberances*. In 50th AIAA Aerospace Sciences Meeting including the New Horizons Forum and Aerospace Exposition, Nashville, Tennessee.
4. Custodio, D., Henoch, C. & Johari, H. (2018) Cavitation on hydrofoils with leading edge protuberances. *Ocean Engineering* 162, pp. 196–208.
5. de Paula, A.A., Meneghini, J.R., Kleine, V.G. & da Mota Girard, R. (2017) *The Wavy Leading Edge Performance for a Very Thick Airfoil*. In 55th AIAA Aerospace Sciences Meeting, doi: 10.2514/6.2017-0492.
6. Dropkin, A., Custodio, D., Henoch, C.W. & Johari, H. (2012) Computation of Flow Field Around an Airfoil with Leading-Edge Protuberances. *Journal of Aircraft* 49 (5), pp. 1345–1355.
7. Fish, F.E. (1999) *Performance Constraints on the Maneuverability of Flexible and Rigid Biological Systems*. Proceedings of the Eleventh International Symposium on Unmanned Untethered Submersible Technology (UUST), UUST99, Autonomous Undersea Systems Inst., Lee, NH, Aug. pp. 394–406.
8. Fish, F.E. & Battle, J.M. (1995) Hydrodynamic Design of the Humpback Whale Flipper. *Journal of Morphology* 225, July, pp. 51–60.
9. Hansen, K.L., Kelso, R.M. & Dally, B.B. (2011) Performance Variations of Leading-Edge Tubercles for Distinct Airfoil Profiles. *AIAA Journal* 49 (1), pp. 185–194.
10. Johari, H. (2012) *Applications of Hydrofoils with Leading Edge Protuberances*. Final Technical Report for Office of Naval Research. Available from: https://apps.dtic.mil/dtic/tr/fulltext/u2/a563228.pdf [Accessed: April 10, 2020].
11. Johari, H., Henoch, C., Custodio, D. & Levshin, A. (2007) Effects of Leading-Edge Protuberances on Airfoil Performance. *AIAA Journal* 45 (11), pp. 2634–2642.
12. Miklosovic, D.S., Murray, M.M., Howle, L.E. & Fish, F.E. (2004) Leading-edge tubercles delay stall on humpback whale (Megaptera novaeangliae) flippers. *Physics of Fluids* 16 (5), pp. L39–L42.
13. Norberg, U.M. (1990) *Vertebrate Flight. Mechanics, Physiology, Morphology, Ecology and Evolutio*. Berlin Heidelberg: Springer-Verlag.
14. Pedro, H.T.C. & Kobayashi, M.H. (2008) *Numerical Study of stall delay on humpback whale flippers*. In 46th AIAA Aerospace Sciences Meeting and Exhibit, Reno, Nevada.
15. Peristy, L., Perez, R., Asghar, A. & Allan, W. (2016) *Reynolds Number Effect of Leading Edge Tubercles on Airfoil Aerodynamics*. In 34th AIAA Applied Aerodynamics Conference, doi:10.2514/6.206-3260.
16. Skillen, A., Revell, A., Pinelli, A. & Piomelli, U. (2015) Flow over a Wing with Leading-Edge Undulations. *AIAA Journal* 53 (2), pp. 464–472.
17. Stein, B. & Murray, M.M. (2005) *Stall Mechanism Analysis of Humpback Whale Flipper Models*. In Proceedings of Unmanned Untethered Submersible Technology (UUST), UUST05, Durham, New Hampshire.
18. User Guide (2020) StarCCM+ version 2020.1. SIEMENS Simcenter.
19. Watts, P. & Fish, F.E. (1999) *The influence of passive, leading edge tubercles on wing performance*. Proceedings of the Eleventh International Symposium on Unmanned Untethered Submersible Technology (UUST), UUST99, Durham, New Hampshire, August, pp. 394–406.
20. Weber, P.W., Howle, L.E., Murray, M.M. & Miklosovic, D. (2011) Computational Evaluation of the Performance of Lifting Surfaces with Leading-Edge Protuberances. *Journal of Aircraft* 48 (2), pp. 591–600.
21. Wu, J.Z., Vakili, A.D. & Wu, J.M. (1991) Review of the physics of enhancing vortex lift by unsteady excitation. *Progress in Aerospace Sciences* 28, 2, pp. 73–131.
22. Zhang, M.M., Wang, G.F. & Xu, J.Z. (2013) Aerodynamic Control of Low-Reynolds-Number Airfoil with Leading-Edge Protuberances. *AIAA Journal* 51 (8), pp. 1960–1971.
23. Zhang, M.M., Wang, G.F. & Xu, J.Z. (2014) Experimental study of flow separation control on a low-Re airfoil using leading-edge protuberance method. *Experiments in Fluids* 55 (4), 1710, doi:10.1007/s00348-014-1710-z.